INTERNATIONAL ATOMIC ENERGY AGENCY
UNITED NATIONS EDUCATIONAL, SCIENTIFIC AND CULTURAL ORGANIZATION
INTERNATIONAL CENTRE FOR THEORETICAL PHYSICS
I.C.T.P., P.O. BOX 586, 34100 TRIESTE, ITALY, CABLE: CENTRATOM TRIESTE

SMR.755/11

Workshop on Fluid Mechanics

(7 - 25 March 1994)

The Atmospheric Boundary Layer

Part II: Temporal and Spatial Variations

D. Etling
Institut für Meteorologie und Klimatologie
Universität Hannover
Herrenhäuser Str. 2
30149 Hannover
Germany

The atmospheric boundary layer
Part II: Temporal and Spatial Variations

D. Etling
Institut für Meteorologie und Klimatologie
Universität Hannover, Herrenhäuser Str. 2
30419 Hannover, F.R.G.

Contents

1 Basic Considerations

Although the atmospheric boundary layer (ABL) is often considered as quasi steady for simplicity, strong temporal variations can be observed in most situations. Lets consider the basic equations for the ABL, which have been derived in detail in Part I. For horizontal homogeneous situations these are the equation of motion

$$\frac{\partial \overline{u}}{\partial t} = +f(\overline{v} - v_g) + \frac{\partial}{\partial z} K_m \frac{\partial \overline{u}}{\partial z} \quad , \tag{1}$$

$$\frac{\partial \overline{v}}{\partial t} = -f(\overline{u} - u_g) + \frac{\partial}{\partial z} K_m \frac{\partial \overline{v}}{\partial z} \quad , \tag{2}$$

and the first law of thermodynamics

$$\frac{\partial \overline{\Theta}}{\partial t} = -\frac{1}{\overline{\rho} c_p} \frac{\partial R}{\partial z} + \frac{\partial}{\partial z} K_h \frac{\partial \overline{\Theta}}{\partial z} \quad . \tag{3}$$

In (1) and (2) u_g and v_g represent the components of the geostrophic wind which are related to the large scale horizontal pressure forces by

$$u_g = -\frac{1}{\overline{\rho} f} \frac{\partial \overline{p}}{\partial y} \quad : \quad v_g = \frac{1}{\overline{\rho} f} \frac{\partial \overline{p}}{\partial x} \quad . \tag{4}$$

In (3) R represents the net radiative fluxes which are the driving forces of the temperature variations.

Temporal variations of wind components u and v and of the potential temperature Θ can be supported by external forces, i.e. u_g, v_g and R or by time changes in the eddy diffusivities for momentum K_m and heat K_h. In absence of variation of the large scale pressure fields, boundary layer winds can change only through influence of thermal stratification on the eddy viscosity K_m.

In other lectures it was shown, that K_m is a function of the Richardson-number, i.e.

$$K_m = f(Ri) \quad , Ri = \frac{g}{\Theta} \frac{\dfrac{\partial \overline{\Theta}}{\partial z}}{\left(\dfrac{\partial \overline{u}}{\partial z}\right)^2} \quad . \tag{5}$$

Temporal variations in K_m and hence in u and v are partly due to the diurnal temperature cycle.

In the following we will consider only these temporal variations in the ABL which are not caused by changing external conditions, i.e. we will assume u_g, v_g = constant.

2 Surface energy balance

For the solution of equation(3) we have to specify boundary conditions, which are usually taken as:

$$\Theta = \Theta_h \quad , z = h \quad ; \Theta = \Theta_0(t) \quad , z = z_0 \tag{6}$$

Θ_h is the temperature at the top of the ABL and is assumed to be constant. At the surface ($z = z_0$), the temperature is a function of time and hence enables temporal variations of the vertical profile $\Theta(z)$. The variation of $\Theta_0(t)$ can be either specified or solved with aid of the so-called energy balance equation (see Pielke (1984) for various methods).

The lower boundary of the ABL and its energy fluxes are shown in Fig. 1. Continuity of energy fluxes at the boundary between the soil layer and the atmosphere is described by the energy-balance equation (see e.g. Oke, 1987):

$$Q^* = Q_E + Q_G + Q_H \tag{7}$$

In (7) Q^* is the net radiation (longwave and shortwave), Q_E is the latent heat flux, Q_H is the sensible heat flux and Q_H the soil heat flux. The net radiative flux Q^* can be resolved by

$$Q^* = \varepsilon\sigma T_0^4 + R_L + R_S \tag{8}$$

where R_L is the long wave radiation from the atmosphere and R_S is the short wave solar radiation. $\varepsilon\sigma T_0^4$ is the outgoing longwave radiation from the earth surface. As $T_0 \approx \Theta_0$, the boundary condition (6) can be prescribed by (7) and (8), but as T_0 is also contained in Q_G and Q_H it can be done only iteratively (see Pielke (1984) for details).

Energy balance equation (7) is related to the surface layer laws (see other lecture notes Part I, Chap. 3 through the heat fluxes by

$$Q_E = \rho L\overline{w'q'} \quad , Q_H = \rho c_p\overline{w'\theta'} \quad . \tag{9}$$

Observations of diurnal variation of the different energy fluxes are shown in Fig. 2 for the case of a moist, bare soil. Other examples can be found in the books of Arya (1988), Oke (1987) and Stull (1988). As a consequence of the variation of surface energy fluxes, temperatures at the surface ($z = z_0$) as well as in the air and in the soil vary with time. This is also shown in Fig. 2 (bottom). Temperature amplitude is largest for the surface temperature T_0 and smallest for the soil temperature T_S.

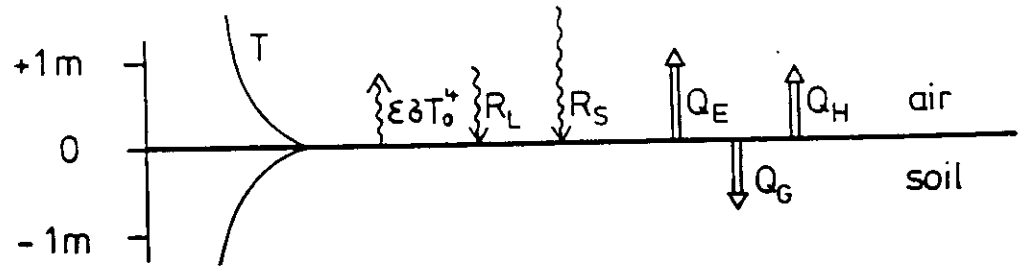

Figure 1: Energy fluxes at the earth's surface (soil-atmosphere interface). Notations like in Eq. (7), (8).

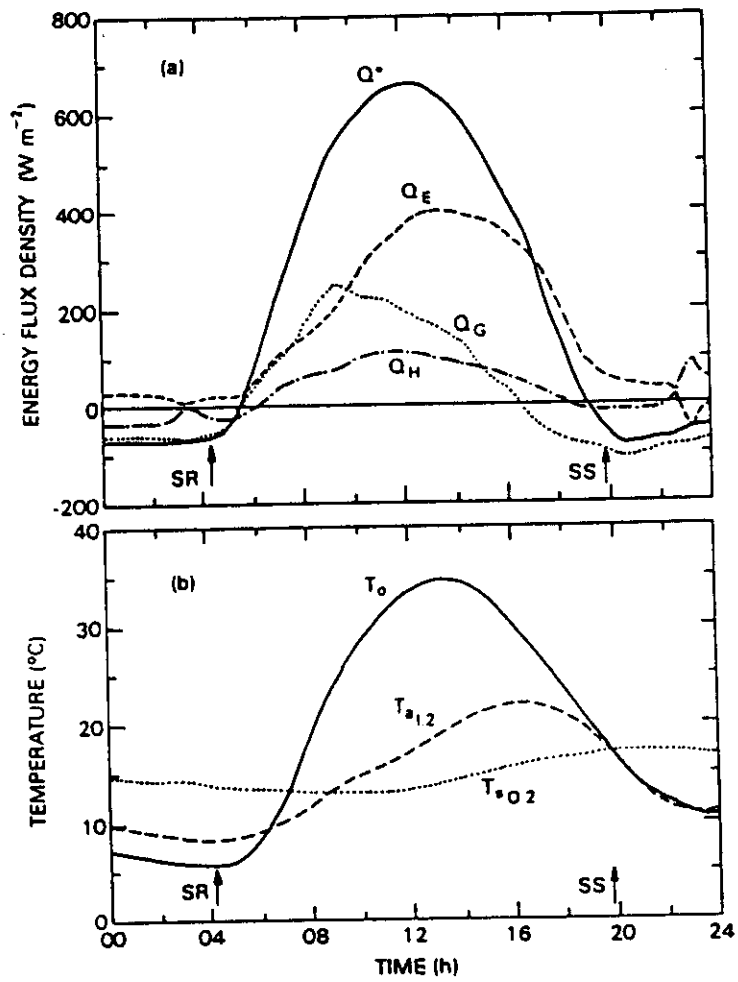

Figure 2: (a): Energy fluxes at the surface over a bare, moist soil. During the course of the day notation as in Eq. (7). (b): Diurnal variation of surface temperature T_0, air temperature T_a at z = 1.2m and soil temperature T_s at z = -0.2m (after Oke, 1987).

3 Temperature variations in the ABL

Diurnal variations of temperature at the surface are transmitted by turbulent diffusion through the ABL (see equation (3)). The typical development of the daytime boundary layer is shown in Fig. 3. The stably stratified temperature profile is eroded away by upward turbulent heat flux after sunrise ending in a so-called mixed layer with nearly uniform temperature.

After sunset, the earth surface is cooled by outgoing longwave radiation leading to a subsequent development of a stably stratified temperature profile (inversion layer) near the ground. One example of a developing nocturnal boundary layer is given in Fig. 4.

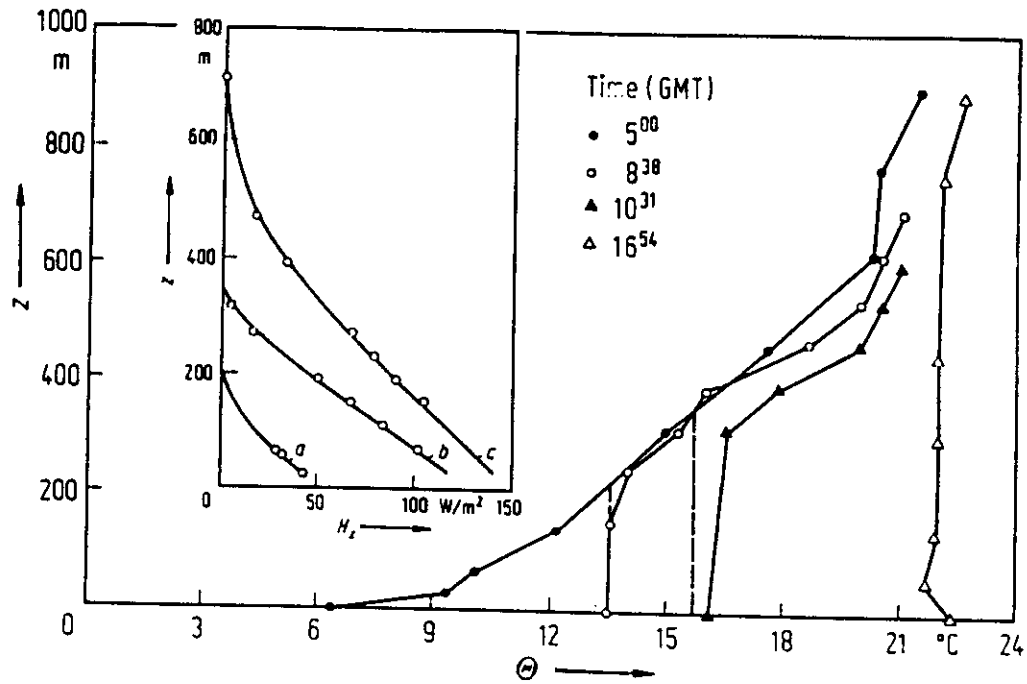

Figure 3: Temporal development of potential temperature Θ in the daytime boundary layer. Profiles of turbulent heat flux $H = \varrho c_p \overline{w'\Theta'}$ are also shown (after Caughey, 1982).

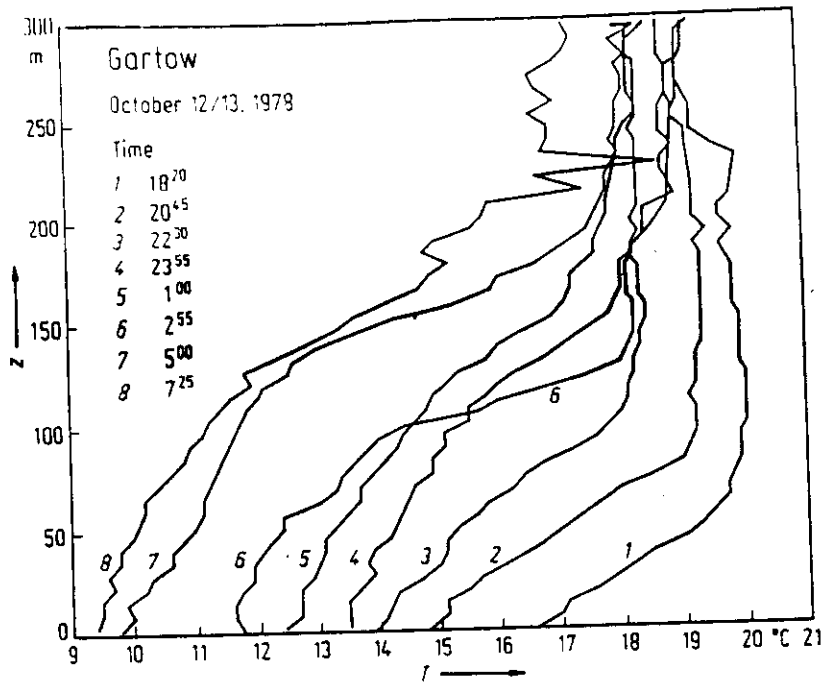

Figure 4: Temporal development of profiles of the temperature T in the nocturnal boundary layer (after Kottmeier, 1984).

4 Wind variations in the ABL

Regarding temporal variations of wind components u and v for the case of constant external forcing (geostrophic wind) these are only possible by variations in eddy viscosity K_m, as can be seen from Eq. (1) and (2). As K_m is related to the temperature profile $\Theta(z)$ by (5), variations in $\Theta(t)$ will lead to temporal variations of the viscosity. Examples of vertical profiles of $K_m(z)$ under daytime and nighttime conditions have already been given in Part I.

Here we will show some results from a numerical model on the variation of K_m during the Wangara field experiment in Fig. 5. Typically, the eddy viscosity is much larger during daytime than during the night as turbulence is enhanced by convection. During nighttime hours, the developing stable stratification (see Fig. 4) is suppressing turbulence. This behaviour of the ABL-structure is shown schematically in Fig. 6.

Observations of wind speed at different heights during the Wangara experiment is shown in Fig. 7 for the course of the day. Near the ground (8m), where usually most routine observations are obtained, wind speed increases during the day due to mixing of high windspeed from above into the surface layer. After sunset wind speed is reduced due to the stable stratification. Both observations are common experience for diurnal wind variations near the ground. In the upper layers of the ABL things are reversed with time, i.e. higher wind speeds are observed during the night and lower wind speeds during the day. This phenomenon is related to the so-called nocturnal jet (low-level-jet) and will be discussed in the next section.

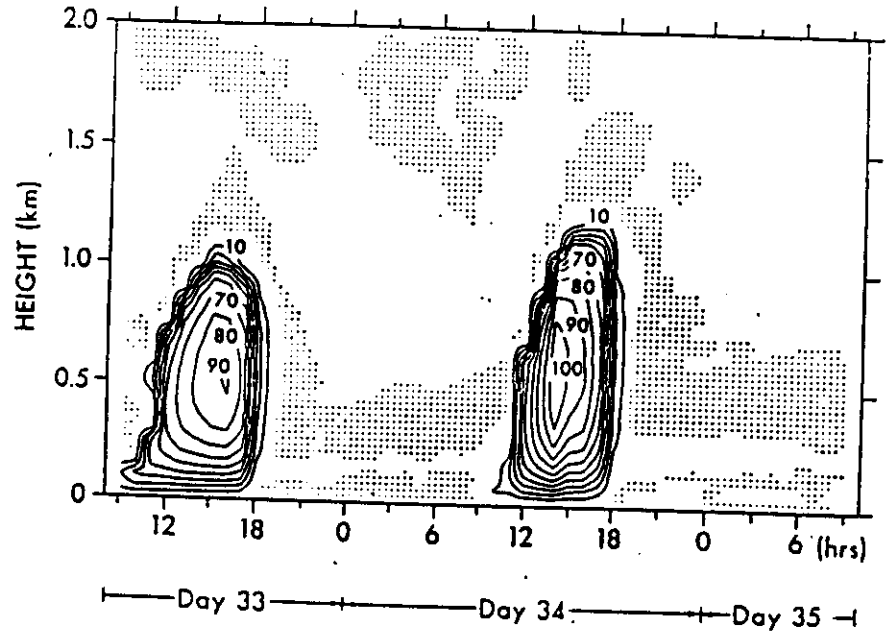

Figure 5: Diurnal variations of the eddy viscosity $K_m(m^2s^{-1})$ during the Wangara experiment (after Yamada and Mellor, 1975).

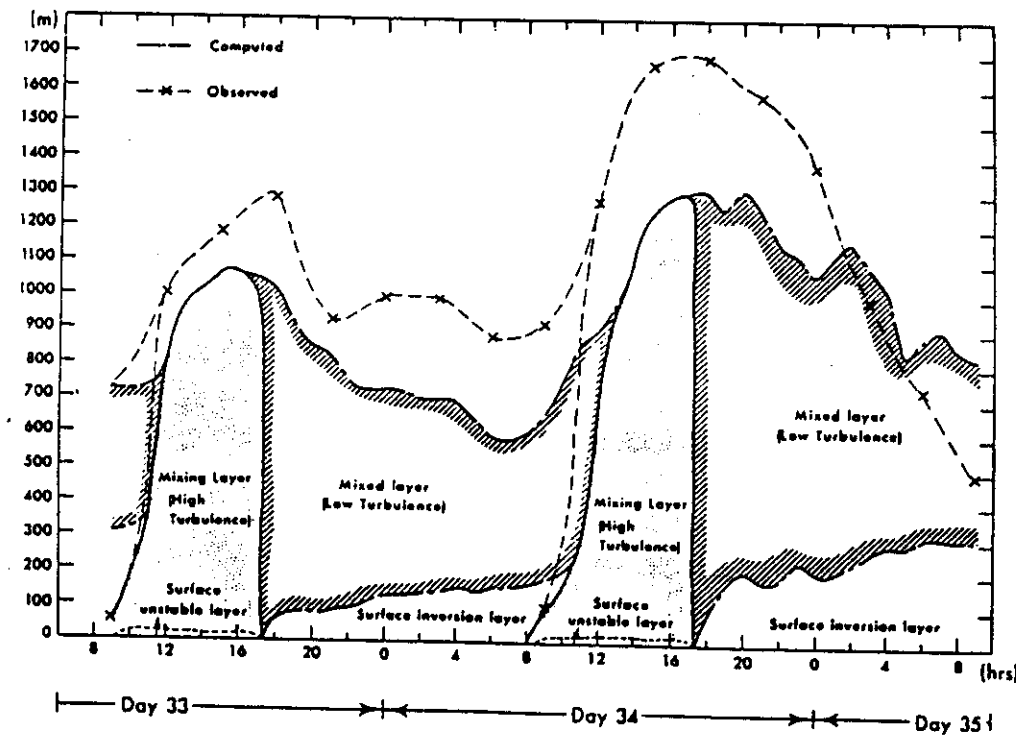

Figure 6: Temporal development of boundary layer height and turbulence state during the Wangara experiment (after Yamada and Mellor, 1975).

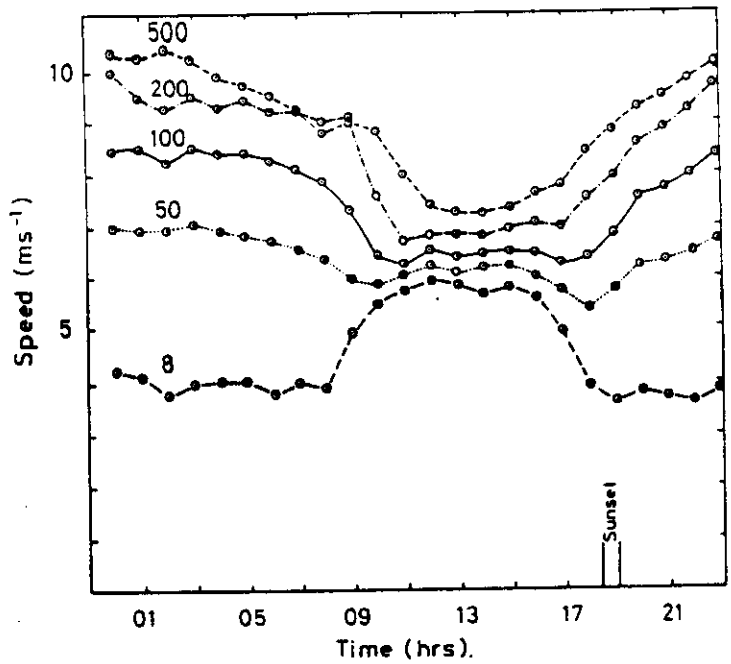

Figure 7: Typical variation of wind speed in the ABL at different heights, lowest level is $z = 8$m (after Mahrt, 1981).

5 The nocturnal low level jet

One specific phenomenon during clear nights is the development of a wind maximum in the lower ABL (say between 100m and 500m), where the wind speed can even exceed the geostrophic wind by 50% or more. This is called a low-level-jet and has been documented intensively by observations (see e.g. Brook (1985) for a recent account). The typical development of a low level jet is shown in Fig. 8.

But not only a variation in wind speed is observed during this phenomenon but also a strong variation in wind direction. This can be seen if the wind components at one specific height are plotted on a so-called wind hodograph, as is shown in Fig. 9.

The development of these oszillations can be described approximately by a theory of Blackadar (1957). After sunset, tubulence is reduced drastically (see e.g. Fig. 5), and hence the frictional forces in Eq. (1), (2) are vanishing. When Pressure, Coriolis and Frictional forces had been in equilibrium before, reduction of friction gives rise to so-called inertial oszillations, as is shown schematically in Fig. 10.

The difference vector $\vec{v} - \vec{v}_g = \Delta\vec{v}$ describes a circular hodograph with radius $(\vec{v} - \vec{v}_g)_0 = \Delta\vec{v}(t = 0)$. It can be described by:

$$\Delta\vec{v}(t) = \vec{v} - \vec{v}_g = \Delta\vec{v}_0 \cos(ft) - \vec{k} \times \Delta\vec{v}_0 \sin(ft) \tag{10}$$

where $\vec{k}$ is the vertical unit vector. The oszillation period τ is defined by

$$\tau = \frac{2\pi}{f} \tag{11}$$

where $f = 2\Omega \sin\varphi$ is the Coriolis parameter as usual. For the latitude of Trieste, for example ($\varphi \approx 46°$), the inertial period is about $\tau \approx 18$ hours.

Now as the initial ageostrophic wind vector $\vec{v} - \vec{v}_g$ is varying with height in the ABL, inertial oszillations with different amplitudes will develope, as is shown in Fig. 11. Therefore there will be some height in the nocturnal ABL, where the supergeostrophic wind will have a maximum value, and a vertical profile of wind speed will show a low level jet.

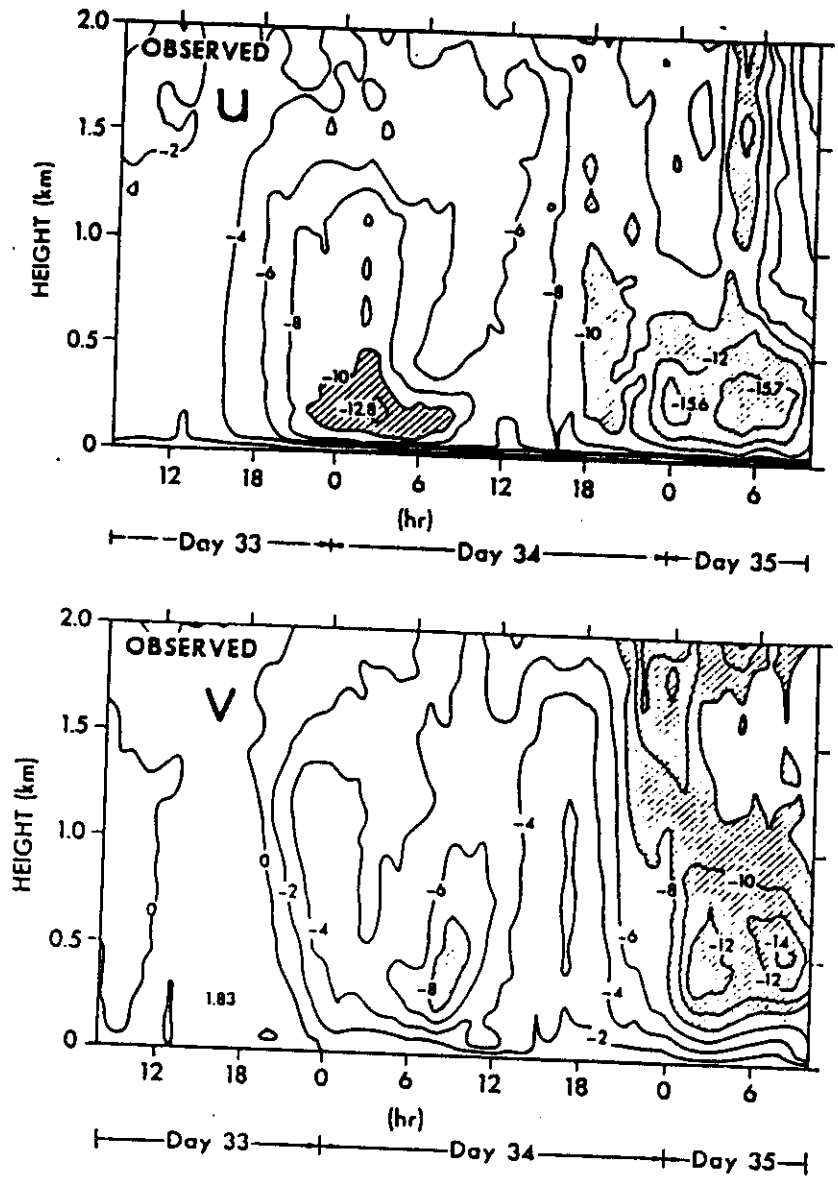

Figure 8: Temporal variation of the wind components u and v during the Wangara experiment. The development of a wind maximum in the lower ABL can be noted during the night (after Yamada and Mellor, 1975).

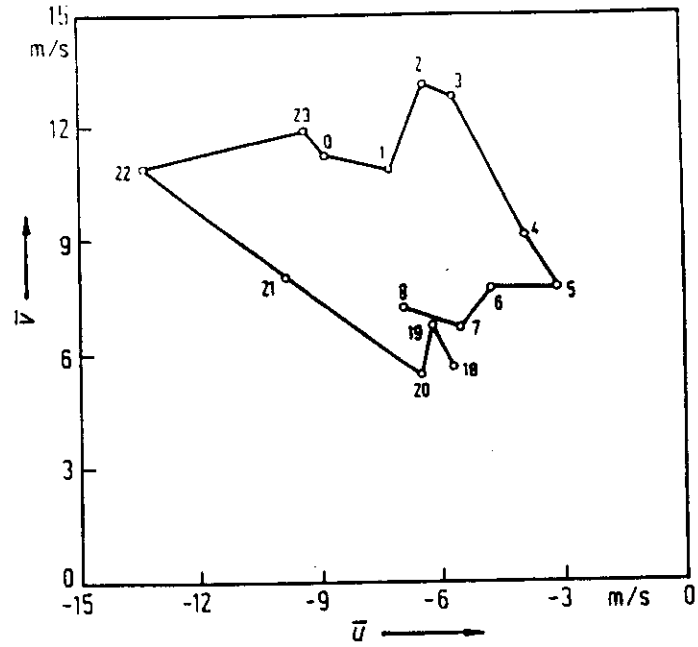

Figure 9: Hodograph of the horizontal wind components u and v at 200m height due to inertial oszillations in the nocturnal boundary layer. Numbers denote time of the day (after Kottmeier, 1984).

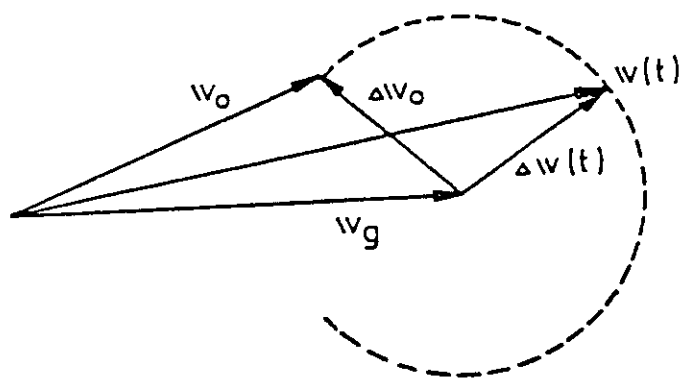

Figure 10: Temporal development of the ageostrophic wind vector $\vec{v} - \vec{v_g} = \Delta\vec{v}$ due to inertial oszillations.

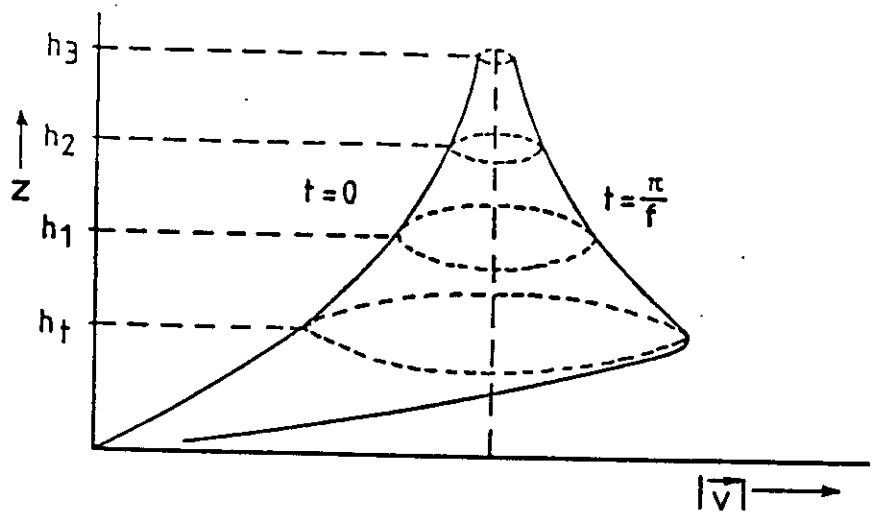

Figure 11: Inertial oszillations in the nocturnal ABL at different heights leading to the development of a low level jet.

6 Spatial variations in the ABL

So far we have assumed, that the ABL is horizontally homogeneous, i.e. there are no variations of wind and temperature in the horizontal directions. This approximation can be only justified, if there are no variations in the conditions of the underlying earth surface. By this we mean a flat terrain of uniform roughness z_0 and homogeneous thermal properties.

In the real world however, these conditions might be found only over parts of the ocean and land surfaces. In most cases the earth surface can be described in terms of non-homogeneous terrain with non-uniform surface properties. Hence the underlying surface has large influence on the development of the ABL and can leed to local flows like sea-breeze, valley winds or topographic wake flows. An example of a sea-breeze circulation is given in Fig. 12. These types of non-homogeneous flows are not treated here but are described in the books of Atkinson (1981), Arya (1988), Oke (1987), Plate (1982), Stull (1988) and Garratt (1992).

Here we will only give a short introduction into the problem of the influence of surface roughness change on the wind profile in the surface layer (chapter 7). As an example of the combined influence of change in roughness and surface temperature on the ABL flow we give some results of numerical simulations of the boundary layer flow over the ice-edge. In Fig. 13 variations of surface stress (u_*^2) and heat flux ($\varrho c_p \overline{w'\Theta'}$) for a flow from continental ice over sea-ice to open water is shown. One can observe drastic changes in both parameters when the air is flowing over the rough sea-ice, where open cracks also give rise to a change in surface temperature (ice and ocean water).

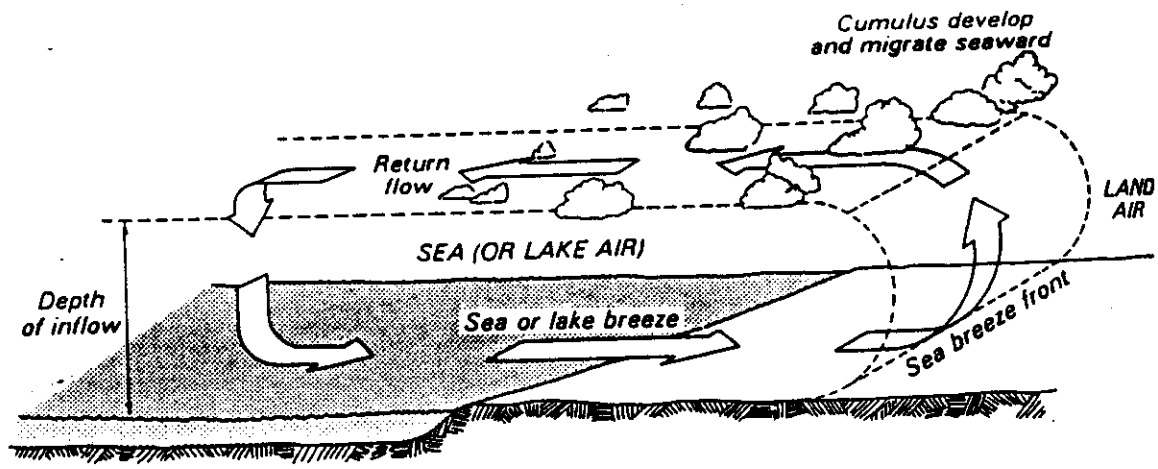

Figure 12: Development of a sea-breeze due to different heating of the land and sea surfaces.

7 Roughness changes in the surface layer

As an example of the influence of surface inhomogeneities on the ABL flow we consider the change of surface roughness length z_0. The typical situation is given in Fig. 14 and might be found for flow from a lake (smooth) to land (rough) or from bare soil (smooth) to a forest canopy (rough). After the air over the upstream roughness z_{01} has reached the new surface with roughness z_{02}, the wind profile is affected from below by the new roughness. The vertical influence reaches up to a height h_i, where upstream and downstream velocities u_1 and u_2 are aproximately equal or say $u_2/u_1 \approx 0.9$.

The layer between the surface and h_i is called Internal Boundary Layer (IBL) and is that part of the surface layer, which is already affected by the new roughness conditions. The height of the IBL h_i increases downstream and can be described approximately by

$$h_i(x) = z_{02} A (x/z_{02})^{0.8} \tag{12}$$

The coefficient A can vary between $A \approx 0.3$ - 0.9, depending on stability (see Arya(1988) or Stull (1988)). For neutral stratification it has also been approximated by

$$A = 0.75 + 0.03\, ln(z_{02}/z_{01}) \tag{13}$$

where z_{01} and z_{02} are the upstream and downstream values of the surface roughness length.

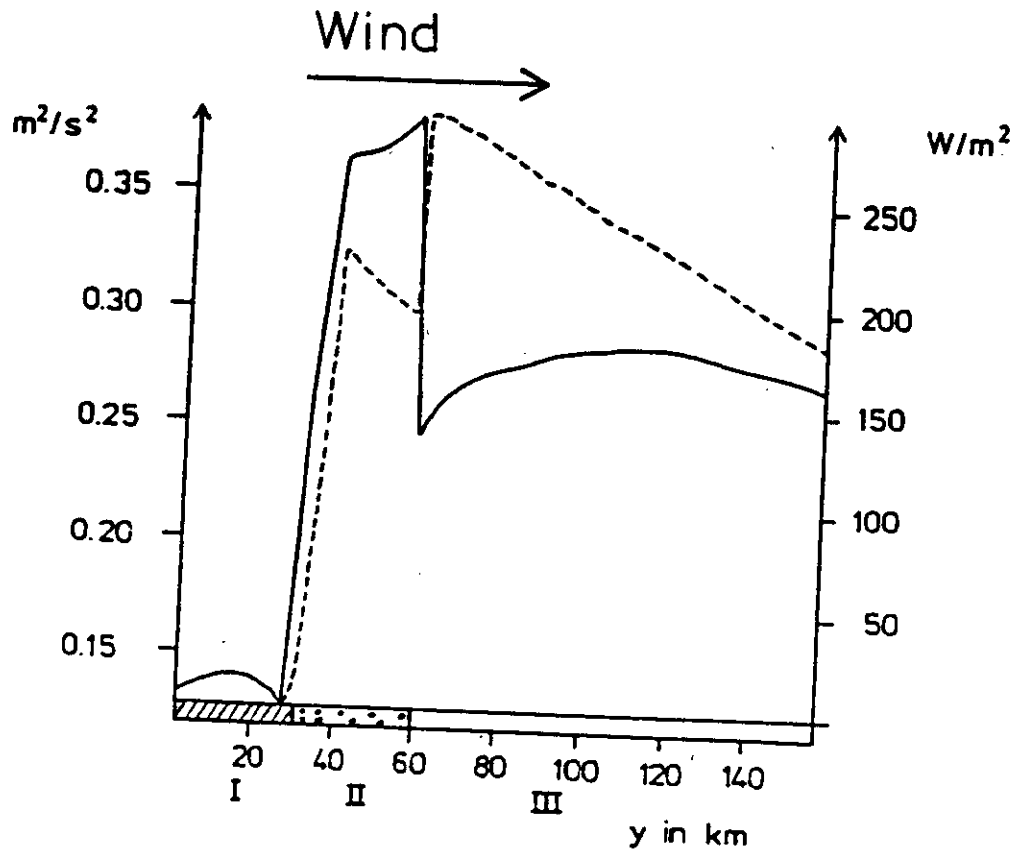

Figure 13: Horizontal variation of surface stress (——) and surface heat flux (- - - -) due to change in roughness and temperature for a flow from ice over sea-ice to the ocean.

Regarding the wind profile, following boundary conditions can be stated for the problem if we assume the usual surface layer approximations (logarithmic wind profile):

$$x < 0 : \overline{u}_1(z) = \frac{u_{*1}}{\kappa} ln \frac{z}{z_{01}} \tag{14}$$

$$x \to \infty : \overline{u}_2(z) = \frac{u_{*2}}{\kappa} ln \frac{z}{z_{02}} \tag{15}$$

Here we have assumed the roughness change at $x = 0$. u_{*2} is the new equilibrium friction velocity downstream of the roughness change. The transition from the upstream windprofile (14) to the new downstream profile (15) is shown from observations in Fig. 15 for a flow from smooth to rough (a) and from rough to smooth (b). The new equilibrium wind profile is attained after a distance $x_e \approx 10^4 - 10^5\, z_{02}$.

For theoretical treatment, the problem can be formulated by a simplified version of the ABL equations for the windspeed u:

$$\overline{u} \frac{\partial \overline{u}}{\partial x} = \frac{\partial}{\partial z} K_m \frac{\partial \overline{u}}{\partial z} \tag{16}$$

which has the form of a classical advection-diffusion equation. Together with inflow condition (14), equation (16) can be solved for $x > 0$ with $z_0 = z_{02}$ as the lower boundary. The eddy viscosity has to be prescribed by some forms as presented in Part I of the lecture or simply by the surface layer profile $K_m = \kappa u_* z$.

Although the roughness change problem has been treated by numerical models (see e.g. Rao et al., 1974), some simple analytic approximations for the development of friction velocity and wind profile have been proposed (see Hunt and Simpson, 1982). These relations may be written as follows:

$$u_{*2}(x) = u_{*1} \left\{ 1 + \frac{ln(z_{02}/z_{01})}{ln(h_i/z_{02})} \right\} \tag{17}$$

$$\overline{u}(z,x) = \frac{u_{*1}}{\kappa} \left\{ ln \frac{z}{z_{01}} - \frac{ln(z_{02}/z_{01})}{ln(h_i/z_{02})} \int_{z/h_i}^{\infty} \frac{e^{-t}}{t} dt \right\} \tag{18}$$

$$h_i(x) = 2\kappa^2 x ln \frac{z_{01}}{h_i} \tag{19}$$

Although Eq. (19) for the IBL height h_i is different from the simple power law (12) and has to be solved by recursion, equations (17)-(19) can give useful estimations of the IBL development without solving a numerical model. Similar analytic solutions for eq. (16), also for the problem of temperature changes due to surface effects, can be found in Sutton (1953).

8 Coherent structures

The atmospheric boundary layer may be termed as a rotating stratified shear flow within the context of fluid mechanics. It is known that these kind of flows can exhibit

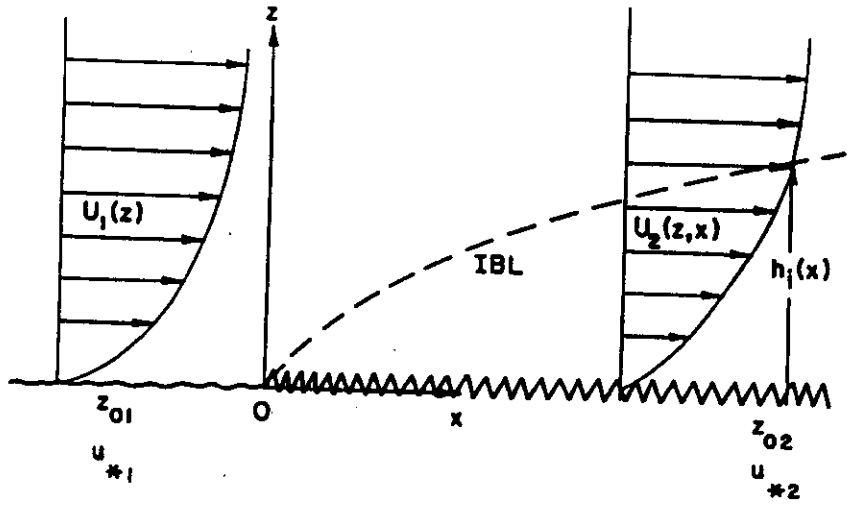

Figure 14: Schematic of the surface layer flow over a step change in surface roughness length z_0.

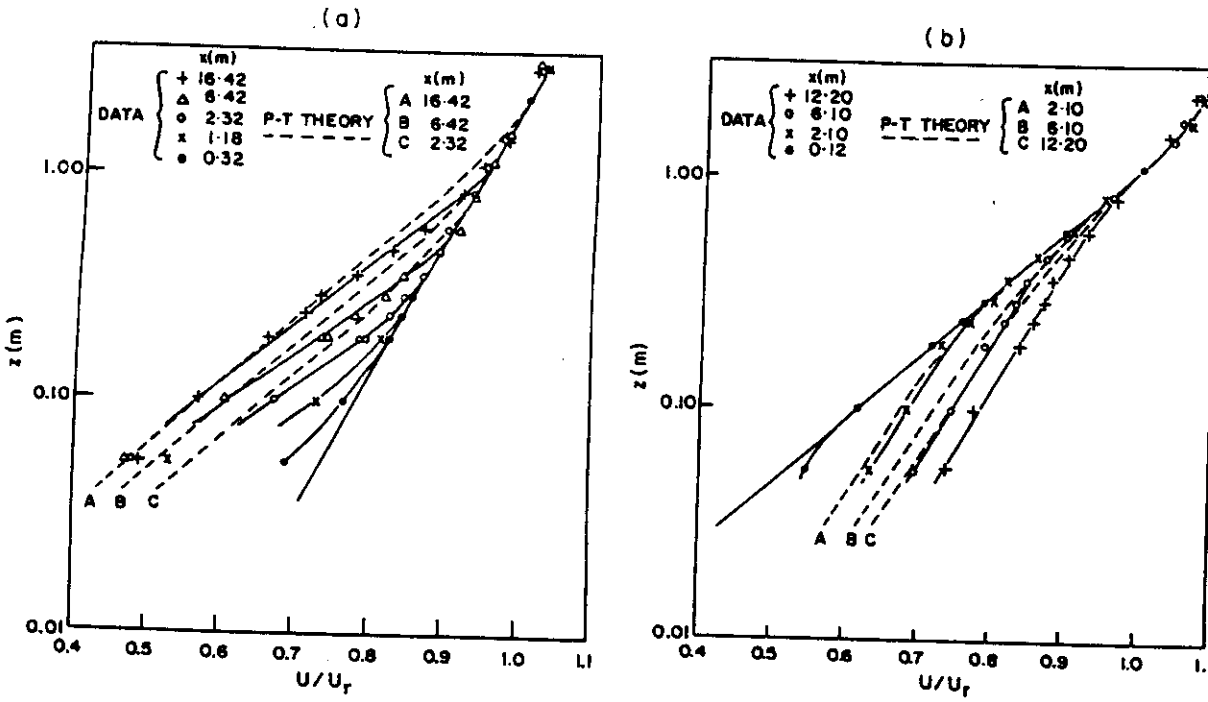

Figure 15: Modification of the wind profile near the ground due to a step change of surface roughness. Solid line (—) denotes upstream wind profile (after Arya, 1988). (a) smooth to rough ($z_{01} < z_{02}$) (b) rough to smooth ($z_{01} > z_{02}$).

various types of instabilities which lead to the formation of large-scale coherent structures. These features can also be observed in the ABL even under homogeneous surface conditions. An example is given in Fig. 16 which shows a satellite picture of clouds formed during a so-called cold air outbreak. The clouds are organized in the form of bands aligned with the mean wind direction. This phenomenon is hence called cloud streets in the literature and can be often observed on high resolution satellite pictures available on a routine basis.

The interpretation of this special type of cloud pattern can be easily achieved by assuming the existence of counter-rotating vortex rolls with axes approximately in the direction of the mean wind, as displayed schematically in Fig. 17. Clouds are formed above the updraft parts of the roll circulations and cloud-free areas are due to sinking motions. These facts have already been known by glider pilots since a long time, as they used this special kind of upward motions as organized in streets for long-distances soaring.

Data evaluation has led to following properties of cloud streets and hence on the roll vortices:

vertical extent	H	1 – 2 km
wavelength	λ	2 – 20 km
aspect ratio	λ/H	2 – 15
downstream extent	E	10 – 1000 km
orientation of roll axis to mean wind	ε	- 20° to + 30°
lifetime	τ	1 – 72 hours

There is a fairly wide range of parameters, especially for the wavelength and the aspect ratio. We will not discuss all of these observations in detail but refer instead to a collection of observations in the review article by Etling and Brown (1993).

With respect to the physical origin of roll vortices in the ABL, two main sources have been identified: thermal instability due to heating of the ground and shear instability due to turning of the wind with height in the ABL. Observations show, that cloud streets are most often formed either during daytime over land or during cold air outbreaks over sea. During the latter, cold air, mostly from polar regions, is advected with the wind over warm ocean surfaces. Hence the ABL is heated from below while the airmass is moving over the ocean. The typical temperature profile during this situation is shown in Fig. 18, where the development of an unstably stratified layer near the ground can be seen. This leeds to Rayleigh-Benard type instability, i.e. rising of warm air and sinking of cold air. As we have a shear flow superimposed on this convective motions, thermal convection will be organized into rolls aligned with the mean shear. This fact is well known from the theory of thermal convection as has been discussed in other lectures of the workshop.

The second kind of instability is more subtile with respect to the cloud street formation. It is related to the so-called inflection point instability, a kind of Kelvin-Helmholtz instability in a non stratified shear flow (see other lectures of the workshop or the book "Hydrodynamic Instability" (Drazin and Reid, 1981). To explain the formation of roll vortices by this instability mechanism, we have to consider the wind profile perpendicular to the roll axis. As can be seen from Fig. 19, the cross flow exhibits an inflection point depending on the orientation of the vortex axis with

the geostrophic wind. This is due to the fact, that in the ABL the wind direction is changing with height due to the action of pressure-, friction and coriolis forces.

Indeed the formation of roll-like vortices in a rotating boundary layer has been well documented in laboratory experiments and is sometimes called Ekman layer instability (see Etling and Brown (1993) for a collection of references).

As it seems now, the mechanism of inflection point instability is responsible for vortex roll formation under near neutral stratification, whereas convective instability is the main source for cloud street development in an unstably stratified ABL. One might consider the formation of cloud streets as a nice example of dynamical and thermal instabilites in geophysical flows. However, in the last decade one has become aware that these special type of organized large eddies play an important role in the vertical transport of momentum, heat, moisture and air pollutants within the PBL.

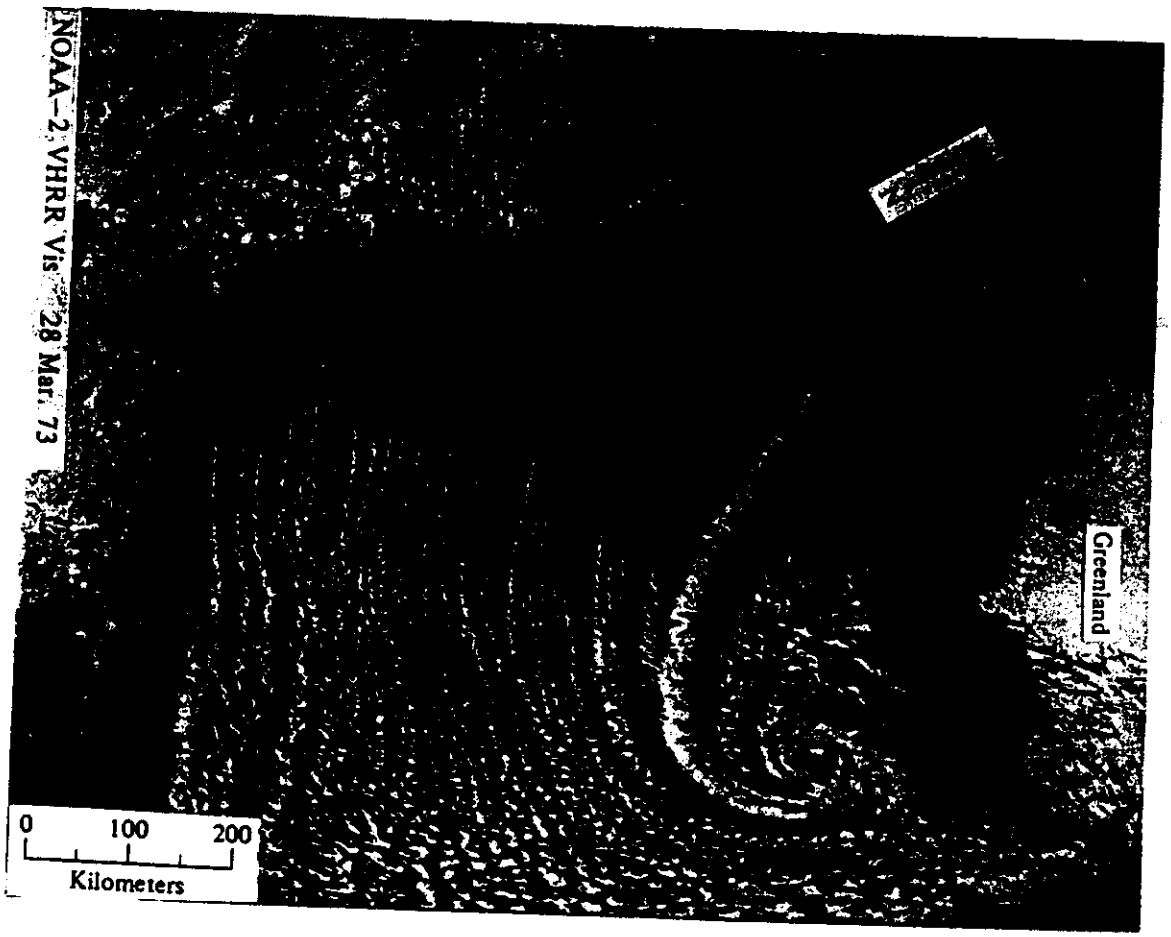

Figure 16: Satellite picture of cloudstreets (white band structures) formed in the ABL over sea during off-shore winds.

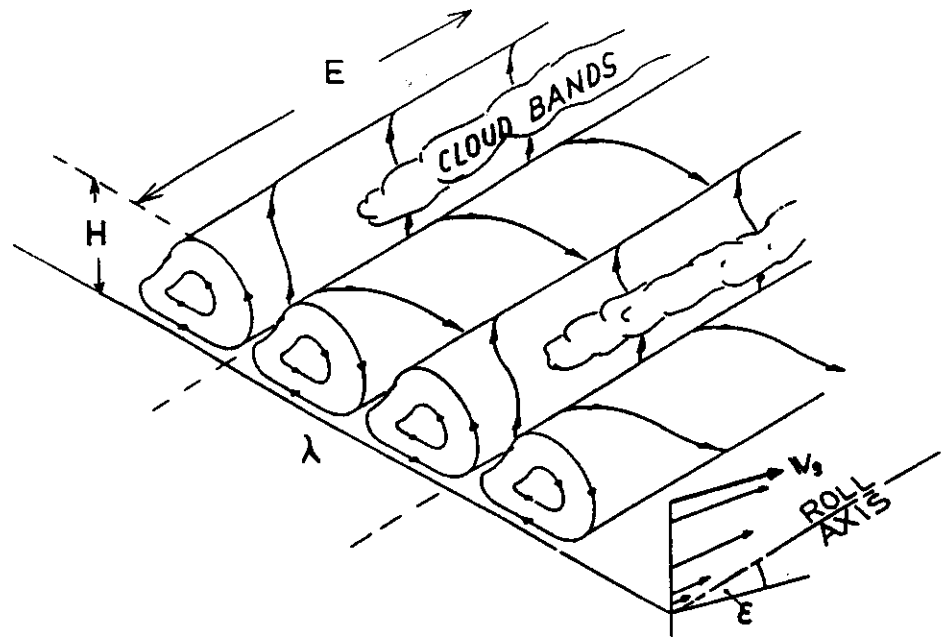

Figure 17: Schematic of organized large eddies (horizontal roll vortices) in the ABL.

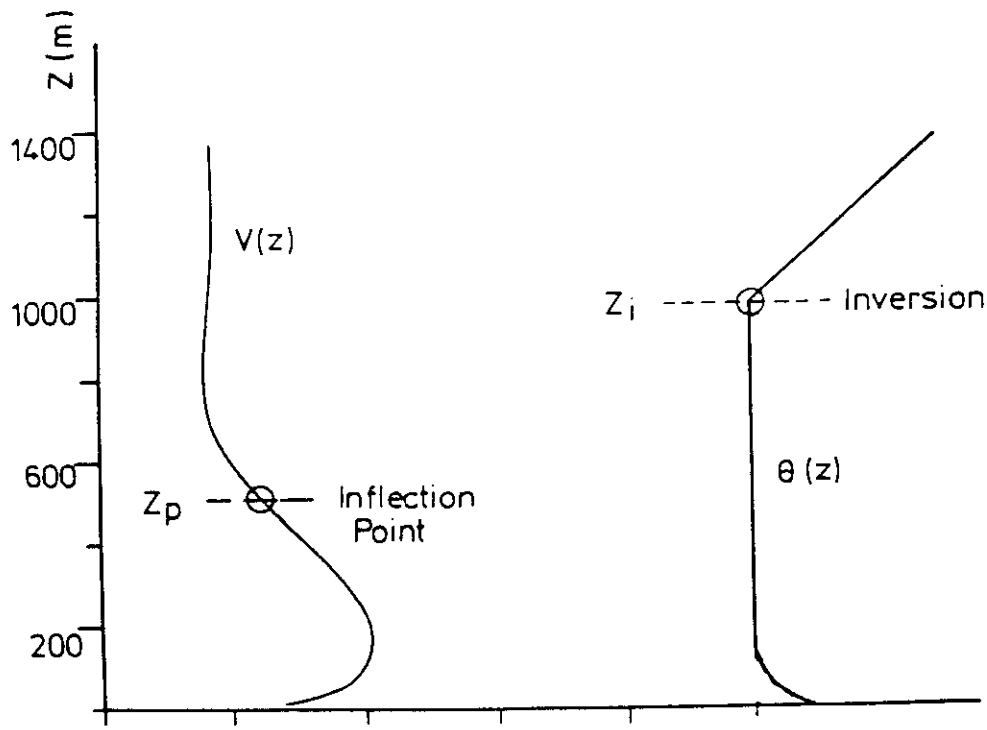

Figure 18: Typical vertical profiles of temperature Θ and cross-roll wind v during cold air outbreaks.

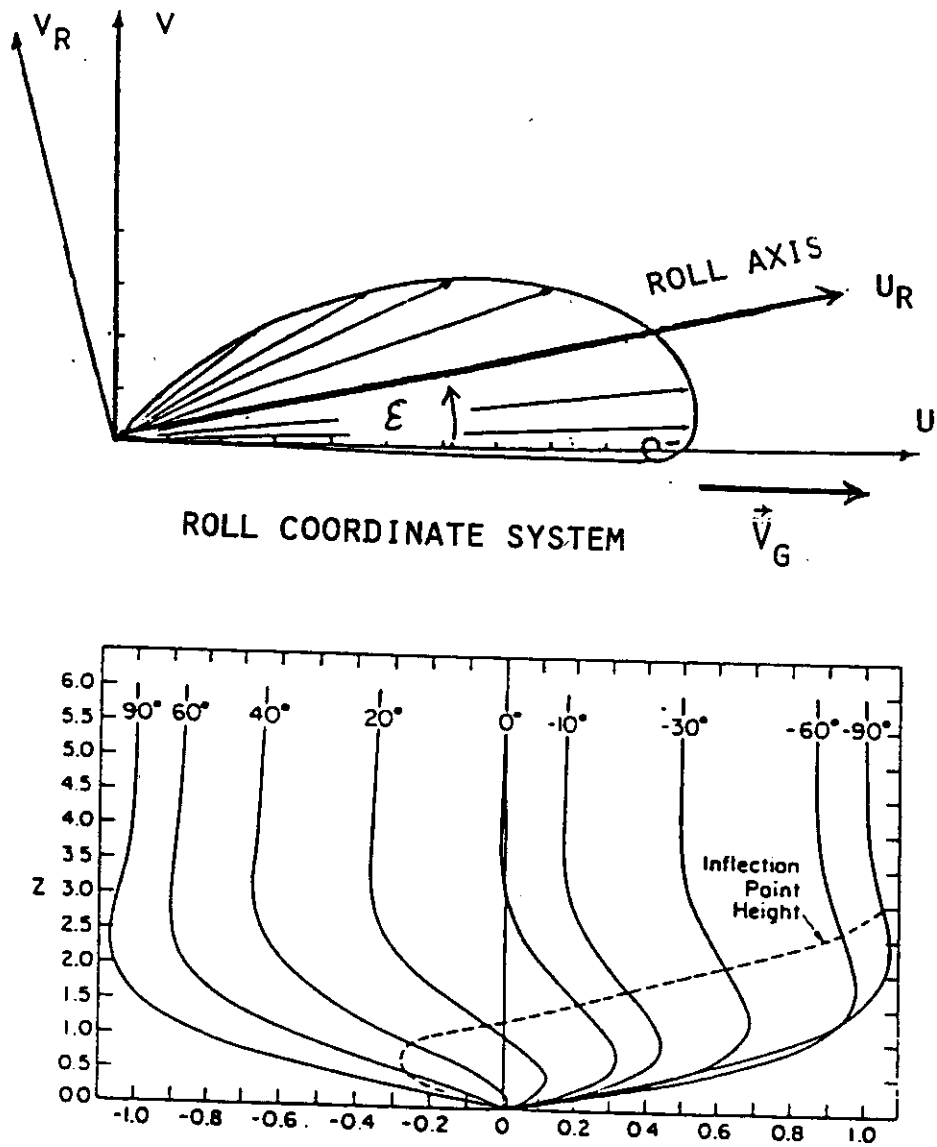

Figure 19: Varation of the cross-roll wind profile V_R for different orientation angle ε between the roll vortex axis and the geostrophic wind. top: Wind hodograph; bottom: cross-roll profile $V_R(z)$.

9 References

Arya, S.P.S. Introduction to micrometeorology. Academic Press, London, (1988).

Atkinson, B.W. Meso-scale atmospheric circulations. Academic Press, London, (1981).

Blackadar, A.K. Boundary layer wind maxima and their significance for the growth of nocturnal inversions. Bull. Am. Met. Soc. 83, 283 - 290, (1957).

Caughey, S.J. Observed characteristics of the atmospheric boundary layer: In: Atmospheric turbulence and air pollution modelling (Nieuwstadt and van Dop, Eds.), D. Reidel, Dordrecht, 107 - 158, (1982).

Drazin, P.G. and Reid, W.H. Hydrodynamic stability. Cambridge University Press, (1981).

Etling, D. and Brown, R.A. Roll vortices in the atmospheric boundary layer: a review. Boundary Layer Meteorol. 65, 215 - 248, (1993).

Garratt, J.R. The atmospheric boundary layer. Cambridge University Press, (1992).

Hunt, J.C.R. and Simpson, J.E. Atmospheric boundary layers over non-homogeneous terrain. In: Engineering Meteorology (Plate, Ed.), Elsevier, Amsterdam, 169 - 318, (1982).

Kottmeier, C. Strukturierte Temperaturprofile bei sehr stabiler Schichtung. Meteorol. Rdsch. 37, 129 - 138, (1984).

Mahrt, L. The early evening boundary layer trasition. Q. J. R. Met. Soc. 107, 329 - 343, (1981).

Oke, T.R. Boundary layer climates. (2nd Edition), Methuen, London, (1987).

Pielke, R.A. Mesoscale meteorological modelling. Academic Press, London, (1984).

Plate, E. Engineering meteorology. Elsevier, Amsterdam, (1982).

Rao, K.S., Wyngaard, J.C. and Cote, O.R. The structure of the two-dimensional internal boundar layer over a sudden change of surface roughness. J. Atmos. Sci. 31, 738 -746, (1974).

Stull, R.B. An introduction to boundary layer meteorology. Kluwer Academic Publ., Dordrecht, (1988).

Sutton, O.G. Micrometeorology. Mc Graw-Hill, New York, (1953).

Yamada, T. and Mellor, G. A simulation of the Wangara atmospheric boundary layer data. J. Atmos. Sci. 32, 2309 - 2329, (1975).